Structure and magnetism of collapsed lanthanide elements

M. I. McMahon,[1] S. Finnegan,[1] R. J. Husband,[1] K. A. Munro,[1] E. Plekhanov,[2] N. Bonini,[2] C. Weber,[2] M. Hanfland,[3] U. Schwarz,[4] and S. G. Macleod[5]

[1]*SUPA, School of Physics and Astronomy, Centre for Science at Extreme Conditions, The University of Edinburgh, Mayfield Road, Edinburgh EH9 3FD, United Kingdom*

[2]*Department of Physics, King's College London, The Strand, London WC2R 2LS, United Kingdom*

[3]*European Synchrotron Radiation Facility, 38043 Grenoble, France*

[4]*Max Planck Institut für Chemische Physik fester Stoffe, Nöthnitzer Straße 40, D-01187 Dresden, Germany*

[5]*Atomic Weapons Establishment, Aldermaston, Reading RG7 4PR, United Kingdom*

(Received 12 March 2019; revised manuscript received 26 June 2019; published 22 July 2019)

Using synchrotron x-ray diffraction, we show that the long-accepted monoclinic structure of the "collapsed" high-pressure phases reported in seven lanthanide elements [Nd, Tb, Gd, Dy, Ho, Er, and (probably) Tm] is incorrect. In Tb, Gd, Dy, Ho, Er, and Tm we show that the collapsed phases have a 16-atom orthorhombic structure ($oF16$) not previously seen in the elements, whereas in Nd we show that it has an eight-atom orthorhombic structure ($oF8$) previously reported in several actinide elements. $oF16$ and $oF8$ are members of a new family of layered elemental structures, the discovery of which reveals that the high-pressure structural systematics of the lanthanides, actinides, and group-III elements (Sc and Y) are much more related than previously imagined. Electronic structure calculations of Tb, combined with quantum many-body corrections, confirm the experimental observation, and calculate that the collapsed orthorhombic phase is a ferromagnet, nearly degenerate with an antiferromagnetic state between 60 and 80 GPa. We find that the magnetic properties of Tb survive to the highest pressures obtained in our experiments (110 GPa). Further calculations of the collapsed phases of Gd and Dy, again using the correct crystal structure, show the former to be a type-A antiferromagnet, whereas the latter is ferromagnetic.

DOI: 10.1103/PhysRevB.100.024107

I. INTRODUCTION

The lanthanide (Ce to Lu) and actinide (Th to Lr) series of metals are characterized by the monotonic increase in the number of their $4f$ and $5f$ electrons, respectively. As electron interactions can be readily modified by changing interatomic distances, studies of the lanthanide and actinide elements under compression have been critical in developing an understanding of f-electron behavior at high densities [1–6]. The f electrons in both series of elements are usually classified as being either localized and characterized by tightly bound shells or narrow bands of highly correlated electrons near the Fermi level or itinerant and able to participate in the metallic bonding [5]. In the predominantly trivalent lanthanides (La to Lu, excluding Ce, Eu and Yb), the $4f$ electrons are localized at ambient conditions, and, on compression, an increase in d-band occupancy resulting from s-d electron transfer gives rise to a common phase-transition sequence between structures comprising different stackings of close-packed layers: hcp- (space-group $P6_3/mmc$ and $hP2$ in Pearson notation) → Sm-type ($R\bar{3}m$ and $hR3$) → double-hcp ($P6_3/mmc$ and $hP4$) → fcc- ($Fm\bar{3}m$ and $cF4$) → distorted-fcc ($R\bar{3}m$ and $hR24$) (Refs. [5,6], and references therein). Although there are no measurable volume changes between any of these different phases, neither do any of them have group-subgroup relationships. Indeed, Porsch and Holzapfel studied the symmetry changes at the $cF4 \rightarrow hR24$ transition in detail and showed that it must be first order [7].

When compressed further, the $hR24$ phases transform to lower-symmetry "collapsed" phases, often via a sudden decrease in atomic volume (Ref. [6], and references therein). Similar behavior is observed in the trans-Pu "heavy" actinide elements (Am [8], Cm [9], and Cf [10]) on compression, each of which transforms via volume discontinuities to complex structural forms seen in the lighter actinides (Th-Pu). Volume discontinuities and the appearance of low-symmetry structures are commonly associated with the pressure-induced delocalization of the $4f/5f$ electrons and their subsequent participation in bonding. However, recent x-ray spectroscopy measurements on Tb to extreme pressure reveal that neither a valence change nor $4f$ delocalization occur at the volume collapse pressure of 53 GPa [11]. Rather, the collapsed phases of both Tb and neighboring Dy exhibit anomalously high magnetic ordering temperatures suggestive of an unconventional magnetic state [12,13]. Understanding the mechanism(s) responsible for these high-ordering temperatures might enable their reproduction in a suitable compound at ambient pressure, leading to the synthesis of superior permanent magnet materials.

The collapsed phases in the regular lanthanides are most commonly reported to have a four-atom monoclinic structure with space-group $C2/m$ ($mC4$ in the Pearson notation) first observed in Ce 40 years ago [16]. Since then, the collapsed phases of Nd, Sm, Gd, Tb, Dy, Ho, Er, and Tm have all been reported to have the same $mC4$ structure (Ref. [6], and references therein) such that it is now *the* key structure in the

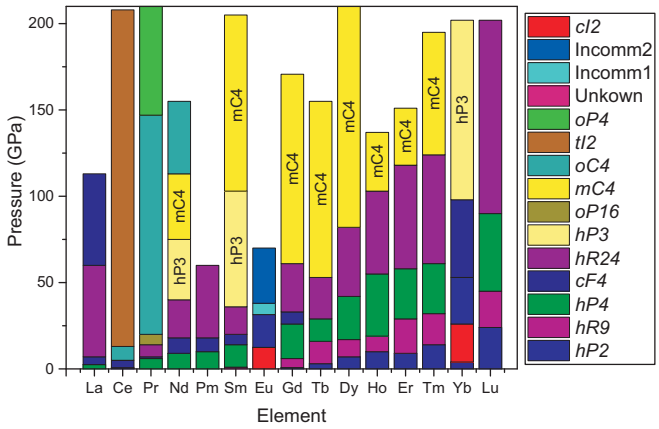

FIG. 1. The different phases reported in the lanthanide elements up to 210 GPa at ambient temperature. Transition pressures are taken from Refs. [6,14,15] and references therein. The collapsed $mC4$ and $hP3$ phases are highlighted in full and pale yellow, respectively, and are labeled. Of the low-symmetry phases, only the $oC4$ and $tI2$ phases are also seen in the actinides.

lanthanide elements at high densities (see Fig. 1). In Nd and Sm, the $mC4$ phase is obtained via an intermediate rhombohedral $hP3$ phase (space-group $P3_121$, but see later) seen only in these two elements [17,18] and Yb [19]. And in Ce, Pr, and Nd, a collapsed phase with the orthorhombic structure found in uranium at ambient conditions (space-group $Cmcm$ and Pearson notation $oC4$) is also found [20–22]; somewhat surprisingly, this and the tetragonal $tI2$ phase seen in Ce and Th [23,24] are the only noncubic crystal structures that the lanthanides and actinides have in common on compression.

There is, thus, a consensus, constructed over decades, as to the structural behavior of the lanthanides on compression as illustrated in Fig. 1 and the phases which are common to both lanthanides and actinides. However, although the similarity of many of the published diffraction patterns from the collapsed phases of the lanthanides suggests they do share a common structure, the widely reported $mC4$ monoclinic structure provides an inadequate fit to many, if not all of them—as detailed in the Supplemental Material [25].

Using high-quality synchrotron x-ray-diffraction data, we have determined the correct structure of the collapsed phase of Tb as orthorhombic with space-group $Fddd$ and 16 atoms per unit cell ($oF16$). Furthermore, we show that the same $oF16$ structure better fits the published diffraction data from the collapsed phases of Dy, Ho, Er, and Tm as well as data we have collected from the collapsed phase of Gd. The $oF16$ structure comprises a stacking of eight quasi-close-packed layers and is isosymmetric with the structures found previously in Pu, Cf, Am, and Cm—although with a four-layer stacking sequence in those cases ($oF8$). We show that the $hP3$ structures of Nd, Sm, and Yb comprise a similar three-layer stacking sequence of the same quasi-close-packed layers, and hence that the $hP3$, $oF8$, and $oF16$ structures form a new family of layered elemental crystal structures, differing only in the stacking sequence of their atomic layers.

The correct determination of the structures of the collapsed phases of Nd, Gd, Tb, Dy, Ho, Er, and Tm greatly strengthens the structural systematics within the lanthanide series, whereas also revealing very much stronger structural links with the actinide elements. Electronic structure calculations using the correct structure for the collapsed phases of Tb, Dy, and Gd provide new insight into the behavior of the $4f$ electrons at high density and provide an explanation for the unusual magnetism seen in the collapsed phases of these elements.

II. EXPERIMENT

We focused our experimental study on the collapsed phase of Tb, which is obtained at a lower pressure (∼50 GPa) than in other lanthanides [26] thereby enabling the highest-quality diffraction data to be collected and which is reported to have an unusual magnetic state [12]. We conducted experiments on two separate Tb samples, reaching a maximum pressure of 110 GPa at 300 K. High-purity distilled samples were loaded into two diamond-anvil cells in a dry argon atmosphere (< 1 ppm O_2 and < 1 ppm H_2O) to prevent oxidation. The first sample was loaded without a pressure medium but with a small piece of Ta foil as a pressure calibrant. The second sample was loaded in a He pressure medium without any pressure calibrant. Diffraction data were collected on the high-pressure ID09 beamline at the European Synchrotron Radiation Facility (ESRF) in Grenoble, (samples 1 and 2) and on the high-pressure I15 beamline at the Diamond Light Source (DLS) in the United Kingdom (sample 1). Monochromatic x-ray beams of wavelength $\lambda = 0.411\,77$ Å (ESRF) and $0.424\,54$ Å (DLS), focused down to a FWHM of 10 μm (ESRF) and 20 μm (DLS) were used, and the powder-diffraction data were recorded on MAR345 (DLS) and Mar555 (ESRF) area detectors, placed ∼350 mm from the sample. The sample pressure in sample 1 was derived from the published Ta equation of state [27], whereas the pressure in sample 2 was determined from the Tb equation of state established using sample 1. The data used to solve the structure were obtained from sample 2. The two-dimensional (2D) diffraction images were integrated using FIT2D [28], and the resulting one-dimensional profiles were analyzed using Rietveld and Le Bail fitting techniques [29] as well as least-squares fitting to the positions of individual diffraction peaks.

III. EXPERIMENTAL RESULTS

On compression, the onset of the transition to the collapsed phase was seen at 54(1) GPa, and single-phase diffraction patterns from it was seen above 64 GPa. The diffraction pattern from Tb at 64 GPa is shown in Fig. 2 with inset (a) showing a Rietveld fit of the reported $mC4$ structure to the midangle region of this profile. This structure completely fails to fit the pattern above $2\theta = 16^\circ$ (see Fig. S1 for the $mC4$ fit to the full profile in the Supplemental Material [25]). In particular, there is a clear doublet at $2\theta = 18^\circ$, the higher-angle peak of which cannot be unaccounted for by the $mC4$ structure. The same doublet is evident in the published diffraction patterns from the collapsed phases of Dy, Ho, Er, and probably Tm (as detailed in the Supplemental Material [25]), whereas the diffraction data we have collected from the collapsed phase of Gd also exhibit the same doublet (Fig. S2 of the Supplemental

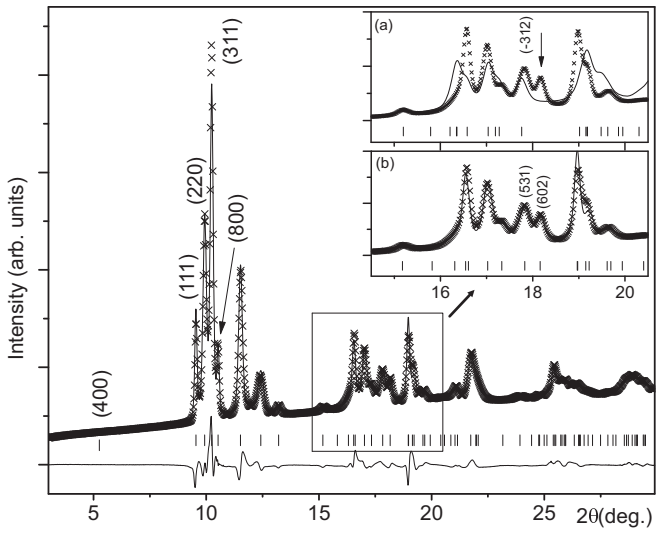

FIG. 2. Rietveld refinement of the *oF*16 structure to the Tb diffraction data at 64 GPa, showing the observed (crosses) and calculated (line) diffraction patterns, the calculated reflection positions (vertical lines), principal Miller indices, and difference profile (lower line). Space-group $Fddd$, Tb on $16e\,(x, 0, 0)$ sites with $x = 3/16$ (fixed), $a = 17.950(2)$, $b = 4.933(1)$, $c = 2.899(1)$ Å. The insets show Rietveld fits to the midangle region of the profile using (a) the *oC*4 structure and (b) the *oF*16 structures. The fit in (a) is clearly very poor, and among other misfits, the *mC*4 structure cannot account for the clear doublet at 18°. The fit provided by the *oF*16 structure is much better, and the doublet arises from the (531) and (602) peaks.

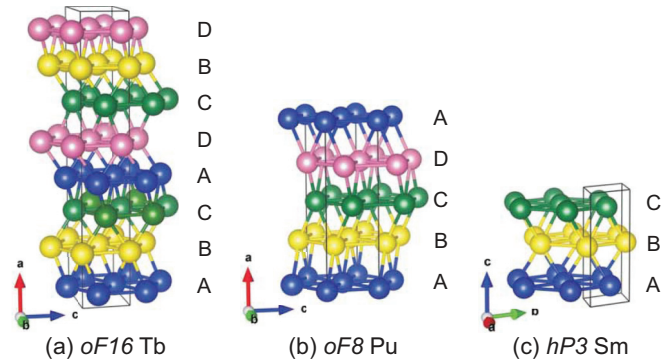

FIG. 3. The *oF*16 structure of Tb at 64 GPa, the *oF*8 structure of Pu at ambient pressure, and the *hP*3 structure of Sm at 47 GPa, all shown on the same scale. The structures each comprise stackings of quasi-close-packed hexagonal planes but with different stacking sequences. In all three structures, the atoms within each layer are stacked over the saddle point of two atoms in the preceding layer, resulting in tenfold coordination. This differs from the stacking of the layers of hcp and fcc, etc., where the atoms are stacked over the midpoint of three atoms in the previous layer and the resulting coordination is 12-fold.

Material [25]). The presence of this doublet shows that *none* of the collapsed phases of Gd to Tm have the long-reported *mC*4 structure.

Ab initio indexing of the Tb data obtained at 64 GPa showed that all of the peaks could be accounted for by an orthorhombic unit cell with $a = 17.950(2)$, $b = 4.933(1)$, $c = 2.899(1)$ Å. The same cell fitted data collected to 110 GPa. The observed peaks and density uniquely identified the space group as $Fddd$ with 16 atoms/cell. Placing the atoms on the 16*e* site at $(x, 0, 0)$ gave an excellent fit with x refining freely to 0.1874(4). The resulting structure comprises eight layers of quasi-close-packed atoms stacked along the a axis. If $x = 3/16 = 0.1875$, then these layers are evenly spaced at $x = 1/16$, $3/16$, etc., and the intensity of the low-angle (400) peak at ∼5° (see Fig. 2) is exactly zero. Lengthy x-ray exposures revealed no evidence of the (400) peak at any pressure, and so we have fixed $x = 3/16$. The final Rietveld refinement with the *oF*16 structure is shown in Fig. 2.

This *oF*16 unit cell is closely related to that of the previously reported *mC*4 cell, which is pseudo-orthorhombic [25] and fits all observed peaks, including the problematic doublet with high precision [see inset (b) in Fig. 2]. The *oF*16 structure also fits our own data from the collapsed phase of Gd [25], and it explains the doublets visible in the reported diffraction patterns from Gd, Ho, Er, and (probably) Tm [25]. The collapsed phases of Gd-Tm, therefore, all have the *oF*16 structures.

The *oF*16 structure of Tb comprises eight quasi-close-packed layers ($b/c \sim \sqrt{(2.9)} \sim \sqrt{3}$) stacked along the a axis [see Fig. 3(a)]. Rather than the stacking seen in fcc, hcp, dhcp, etc., where atoms in the close-packed layers are located above the midpoint among three atoms in the previous layer, in the *oF*16 structure, the atoms are located above the saddle point between two atoms in the previous layer. This results in tenfold $(6 + 2 + 2)$ coordination, and the possibility of each layer to choose among three different positions relative to the previous layer. As a result, the *oF*16 structure of Tb has an eight-layer ABCADCBD repeat. Exactly the same type of layer stacking is seen in the isosymmetric *oF*8 structure of Pu (which is also seen in Am, Cm, and Cf on compression [8–10]), although this structure has only a four-layer ABCD repeat [Fig. 3(b)].

It is possible to predict other members of the same structural family, such as structures having three-layer (ABC) or six-layer (ABCADC) stacking sequences. Analysis of the *hP*3 structure reported in Nd, Sm, and Yb shows that this is the three-layer ABC structure [Fig. 3(c)] [30]. We note that the *hP*3 phase of Nd has recently been reported to exhibit the same rapid increase in magnetic ordering temperature seen in the *oF*16 phases of Tb and Dy [31], whereas the ordering temperature in *hP*3-Sm is relatively unchanged with pressure [32].

Furthermore, the monoclinic phase of Cm-III (space-group $C2/c$), which is stabilized by spin polarization of its $5f$ electrons, has a very similar structural motif to *hP*3 [9], whereas the structure of Sc found above 240 GPa is only slightly distorted from *hP*3 [33]. The collapsed phases of the regular trivalent lanthanides, divalent Yb, Pu at ambient pressure and high temperature, Am, Cm, and Cf on compression, and Sc at extreme pressures are, thus, all members of this new family of elemental structures. The six-layer ABCADC structure, and other possible members, remain to be identified.

The *oF*16 structure has not been reported previously in the elements, but was predicted to be a high-pressure form of Y, with the *oF*16 and *hP*3 phases being energetically favorable at pressures over 97 GPa [34]. Although the similarity in the enthalpies of these two structures is perhaps not surprising given the structural similarities revealed here, the same calculations showed that the *oF*8 form of Y would have a somewhat higher enthalpy and was unlikely to be observed. We note that the experimentally determined structure of collapsed Y above 100 GPa is the same *mC*4 structure of collapsed Tb, etc. [35]. New data are required to determine whether this phase too has the *oF*16 structure, which would further strengthen the structural systematics of Y and Sc with those of the lanthanides and actinides.

Finally, we address the structures of the collapsed *mC*4 phases of Nd and Sm which are obtained via a transition from the lower-pressure *hP*3 phase (Fig. 1). The diffraction patterns of *mC*4-Nd [36] and *mC*4-Sm [37] are both very different from each other and from those reported in the higher-*Z* lanthanides. The lattice parameters of *mC*4-Nd and *mC*4-Sm are also very different ($\beta = 118.6^\circ$ in Nd at 89 GPa [36], and $\beta = 112.8^\circ$ in Sm at 109 GPa [37]). However, the published diffraction pattern from *mC*4-Nd is strikingly similar to that reported for *oF*8-Am [8], and there is a clear relationship between the *mC*4 and the *oF*8 unit cells [25]. As a result, Nd at 89 GPa can be fitted with the *oF*8 structure of γ-Pu with $a = 2.7160(1)$, $b = 4.8473(2)$, and $c = 8.8618(2)$ Å [25]. The $P6_222$ and $Fddd$ space groups of *hPd*-Nd and *oF*8-Nd are not group-subgroup related, but the previous determination of the equation of state of Nd to 155 GPa [22] revealed that there is no volume discontinuity at the $hP3 \rightarrow oF8$ transition, a result which, due to the close similarities of the lattices of the *mC*4 and *oF*8 structures [25], is unaffected by whether the higher-pressure phase is indexed as orthorhombic or monoclinic.

This first observation of the *oF*8 structure in a lanthanide element further strengthens the structural similarities of the lanthanide and actinide series and reveals that the three-, four-, and eight-layer structure types are all observed in the lanthanide elements. Further studies will be required to determine the true structure of the post-*hP*3 phase of Sm, which has recently been shown to exhibit the rapid increase in magnetic ordering temperature seen in the *oF*16 phases of Tb and Dy [32].

IV. ELECTRONIC STRUCTURE CALCULATIONS

The calculations of Chen *et al.* on Y showed that the shift of the *d*-electron energy levels and *s*-to-*d* electron transfer gave rise to the stability of the *oF*16 and *hP*3 structures. As Y has no *f* electrons, their role in stabilizing the *oF*16 structure in the lanthanides was undetermined. To address this, we have performed extensive density-functional theory (DFT) and dynamical mean-field theory (DMFT) calculations of the *oF*16 phases of Tb, Gd, and Dy.

Structural optimization of bulk Tb in the *mC*4 and *oF*16 phases was accomplished by using spin-polarized DFT calculations with the help of the VASP [38] package using the Perdew-Burke-Ernzerhof functional [39]. The many-body properties of the *mC*4 and *oF*16 phases were further investigated by using a recent implementation of DFT + DMFT in the CASTEP code [40–42]. The *k*-point sampling was performed using a Monkhorst-Pack mesh of $8 \times 8 \times 8$ for the *oF*16 and $10 \times 10 \times 6$ for the *mC*4 structures, respectively, and a Gaussian smearing of 0.1 eV. Convergence in DFT over the *k* points was achieved within 1 meV per atom, and the energy cutoff was 800 eV. Scalar relativistic spin-orbit coupling was taken into account within the Koelling-Harmon approximation [43].

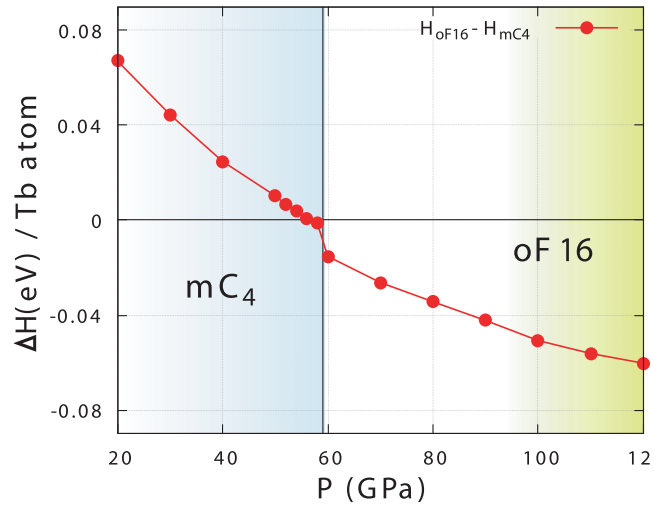

FIG. 4. The enthalpy difference per Tb atom as a function of pressure as predicted by magnetic DFT. The calculations were performed at 0 K.

In the DMFT, we used the Hubbard I solver, valid for *f* elements. In this paper, we focused on the DMFT approach within the framework of fixed Kohn-Sham potentials, the so-called "one-shot" DFT + DMFT method. This has been shown to predict the equilibrium volume and bulk modulus for *f* materials that are in excellent agreement with experimental data [40]. We use typical values for the Coulomb repulsion ($U = 6$ eV) and Hund's coupling ($J = 1$ eV). Throughout this paper, we performed DFT + DMFT calculations with fixed charge and used the fully localized limit type of double-counting corrections.

Zero-temperature DFT calculations for Tb confirmed that the *oF*16 phase is stable with respect to *mC*4 above 60 GPa (see Fig. 4), and the predicted atomic volume of the *oF*16 phase is in good agreement with the room-temperature experimental data. Calculations of the phonon spectrum of *oF*16-Tb at 80 GPa (see Fig. S6 of the Supplemental Material [25]) structure verified its stability (no soft phonons). We see no evidence of the *mC*4 phase at any pressure in our (room-temperature) diffraction studies. The ground states of both the *mC*4 and the *oF*16 phases are calculated to be ferromagnetic, but in the *oF*16 phase between 60 and 80 GPa, the energy difference between the ferromagnetic and antiferromagnetic (AF) state is on the order of room temperature, suggesting that competition between these different magnetic states might occur in this pressure range. This may account for the highly nonmonotonic behavior of the magnetic ordering temperature observed in Tb near 70 GPa by Lim *et al.* [44]. Remarkably, the AF phase in Tb is stabilized via a gain of internal electronic energy but at the cost of a lattice expansion. This

rules out the possibility for AF order at higher pressures. In Gd, however (see the discussion below), the AF order is concomitant with a reduction of the volume and, hence, is naturally stabilized at higher pressures.

We emphasize that the remarkable agreement between theory and experiments can only be achieved within spin-polarized DFT which accounts for the strong magnetic moments due to f electrons: The simpler nonmagnetic DFT approach does not provide a reasonable equation of state, confirming the importance of magnetism for the structural properties above 60 GPa. Indeed, the volume obtained at 60 GPa in nonmagnetic calculations is 14% lower than the experimental value, whereas magnetic calculations calculate the atomic volume to within 1.5% of the experimental value.

Although the magnetism in Tb is not stable at room temperature, at which our experiments have been carried out, a local fluctuating magnetic moment due to f states is expected to persist in the paramagnetic state at 300 K. It is, therefore, important to properly describe the dynamical fluctuations of local magnetic moments within the theoretical framework, which is not achievable within DFT calculations and requires extensions.

For this, we carried out DFT + DMFT calculations at room temperature. Figure 5 shows the calculated spectral weight in the paramagnetic DFT + DMFT solution. Although the DMFT approximation does not have long-range magnetic order, it describes the fluctuations of the local magnetic moment of the Tb atoms. Note that, in DMFT, we observe sharp resonances corresponding to the splitting of the f states into magnetic multiplets [see Fig. 5(a)] with the majority spin states at -5 eV and the minority spin states at $+7$ eV.

Additionally, we also obtain a sharp peak at the Fermi level [at $\omega = 0$, see Fig. 5(a)]. This narrow feature is absent at simpler levels of approximations (such as DFT), and, although it does not impact on averaged quantities, such as forces or magnetism, it sheds light on possible emerging excitations, important for thermomechanical constants and specific-heat coefficients.

The picture of the collapsed phase of Tb that emerges from our calculations is that of a lattice of unscreened weakly coupled local moments embedded in a delocalized d-conduction band with a large bandwidth. As discussed in the DFT context, the unscreened moments are key for the correct description of the structure at high pressure. On compression (see Fig. S5 in the Supplemental Material [25]), we observe only minor changes in the overall spectral weight, and the magnetic moment remains a sextet $S = \frac{5}{2}$ at all pressures studied.

Our finding that the collapsed phases of Dy and Gd also have the $oF16$ structures prompted us to expand our DFT calculations to these two elements, which are reported to exhibit different magnetic behaviors under pressure [44]. At 90 GPa and 0 K, our calculations confirm the $oF16$ phase is energetically favorable compared to the $mC4$ phase in both Dy and Gd—although, in Gd, the $mC4$ phase is calculated to be more stable below 90 GPa. Our room-temperature diffraction studies of Gd see no evidence of the $mC4$ phase at any pressure.

At 90 GPa and 0 K, $oF16$-Gd is calculated to be a type-A antiferromagnet, whereas $oF16$-Dy is calculated to be a ferromagnet. This contrasts with the results for Tb which identify it as a Kondo ferromagnet, nearly degenerate with an antiferromagnetic state between 60 and 80 GPa. Our calculations show that the magnetic order in Dy is much more robust than in Tb and Gd, in agreement with the higher magnetic ordering temperature observed by Lim *et al.* [44]. Indeed, the enthalpy difference in Dy between the ferromagnetic and antiferromagnetic states is 0.14 eV/atom, whereas in Tb and Gd it is $\approx |0.06|$ eV/atom at 110 GPa.

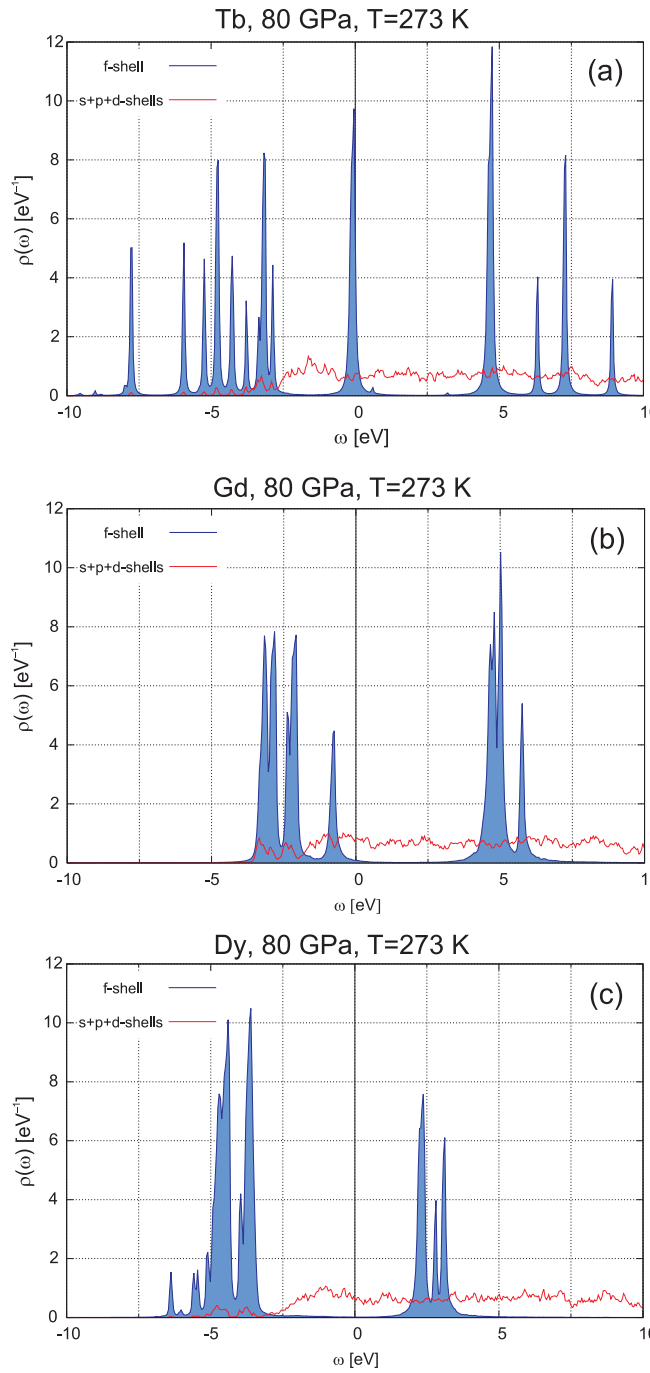

FIG. 5. DMFT spectral weight $\rho(\omega)$ obtained at room temperature and 80 GPa for the $oF16$ phases (a) Tb, (b) Gd, and (c) Dy. The sums of the s, p, and d orbitals are shown in red, and the sums of the f orbitals are shown in blue.

For all three elements, the spin magnetic moment of the f shell persists at room temperature at 80 GPa—$S = 3\mu_B$ in Gd, $S = 2.5\mu_B$ in Tb, and $S = 2\mu_B$ in Dy, although the long-range magnetic order is lost. These magnetic moments are approximately $0.5\mu_B$ smaller as compared to the respective free ions due to the transfer of approximately one electron from the f shell to the d shell as a consequence of applied pressure. However, the different magnetic behaviors of the materials can be inferred by their different paramagnetic properties. In particular, as antiferromagnetism is stablized by Ruderman-Kittel-Kasuya-Yosida processes [45,46] mediated by conduction electrons, the hybridization between f and d states is key to obtaining antiferromagnetic order. Our calculations reveal that the f and d states are indeed hybridized in Gd [see Fig. 5(b)], whereas such hybridization is absent in Dy [see Fig. 5(c)]. Indeed, in Dy, the f states are below the Fermi level (between -7 and -3 eV) and are very weakly hybridized to the d states as the weight of these states is weak in this energy window [see the red curve in Fig. 5(c) between -7 and -3 eV).

V. CONCLUSIONS

The assignment of the *oF*16 structure to the collapsed phases of Tb, Gd, Dy, Ho, Er, and Tm rewrites the long-established structural systematics of the lanthanide elements, whereas the *oF*16 structure's close similarity to the isosymmetric *oF*8 structure seen in Pu, Am, Cf, and Cm reveals a previously unrecognized relationship between the high-pressure phases of the lanthanide and actinides series. This is reinforced further by the discovery that the highest-pressure phase of Nd also has the same *oF*8 structure and that the *oF*16 and *oF*8 structures and the *hP*3 structure found in Nd, Sm, and Yb, are all members of a new family of elemental crystal structures. Further members of this family are predicted and remain to be discovered.

State-of-the-art quantum many-body calculations using the correct structure for the collapsed phase provide new insights into the physics of f elements at high pressure and, in particular, highlight that Kondo-type physics, and more generally magnetism, can be sustained at extreme pressure, a question that has long eluded scientists of the field as emergent quantum phenomena, such as the Kondo effect, are associated with exponentially low-energy scales. The joint experimental and theoretical approach confirms that magnetism of the $4f$ electrons is correctly accounted for, and a classification of typical lanthanides has been obtained in terms of ferromagnetism, antiferromagnetism, and Kondo behaviour for Dy, Gd, and Tb, respectively. The interplay between structural properties and electronic properties accounts for the stability of antiferromagnetism in Gd, absent in Tb.

Note added in Proof. New diffraction data from the collapsed phases of Sm at 175 GPa and Y at 125 GPa suggest that they have the *oF*8 and *oF*16 structures, respectively [54].

ACKNOWLEDGMENTS

©British Crown Owned Copyright 2019/AWE. Published with permission of the Controller of Her Britannic Majesty's Stationery Office. This work was supported by Grants (Grants No. EP/R02927X/1 and No. EP/R02992X/1) from the U.K. Engineering and Physical Sciences Research Council (EPSRC) and facilities made available by the European Synchrotron Radiation Facility and Diamond Light Source. We thank D. Daisenberger and A. Kleppe for their support on the I15 beamline. M.I.M. is grateful to AWE for the award of a William Penney Fellowship. The computational work was supported by the ARCHER U.K. National Supercomputing Service and the U.K. Materials and Molecular Modeling Hub for computational resources (EPSRC Grant No. EP/P020194/1).

[1] U. Benedict, W. A. Grosshans, and W. B. Holzapfel, Physica B & C **144**, 14 (1986).
[2] W. B. Holzapfel, Physica B **190**, 21 (1993).
[3] W. B. Holzapfel, J. Alloys Compd. **223**, 170 (1995).
[4] K. Gschneidner, J. Alloys Compd. **223**, 165 (1995).
[5] B. Johansson, Hyperfine Interact. **128**, 41 (2000
[6] G. K. Samudrala and Y. K. Vohra, in *Handbook on the Physics and Chemistry of Rare Earths*, edited by J.-C. G. Bünzli and V. K. Pecharsky (Elsevier, Amsterdam, 2013), Vol. 43, pp. 275–319.
[7] F. Porsch and W. B. Holzapfel, Phys. Rev. B **50**, 16212 (1994).
[8] S. Heathman, R. G. Haire, T. Le Bihan, A. Lindbaum, K. Litfin, Y. Méresse, and H. Libotte, Phys. Rev. Lett. **85**, 2961 (2000).
[9] S. Heathman, R. G. Haire, T. Le Bihan, A. Lindbaum, M. Idiri, P. Normile, S. Li, R. Ahuja, B. Johansson, and G. H. Lander, Science **309**, 110 (2005).
[10] S. Heathman, T. Le Bihan, S. Yagoubi, B. Johansson, and R. Ahuja, Phys. Rev. B **87**, 214111 (2013).
[11] G. Fabbris, T. Matsuoka, J. Lim, J. R. L. Mardegan, K. Shimizu, D. Haskel, and J. S. Schilling, Phys. Rev. B **88**, 245103 (2013).
[12] J. Lim, G. Fabbris, D. Haskel, and J. S. Schilling, Phys. Rev. B **91**, 174428 (2015).
[13] J. Lim, G. Fabbris, D. Haskel, and J. S. Schilling, Phys. Rev. B **91**, 045116 (2015).
[14] R. J. Husband, I. Loa, G. W. Stinton, S. R. Evans, G. J. Ackland, and M. I. McMahon, Phys. Rev. Lett. **109**, 095503 (2012).
[15] R. J. Husband, I. Loa, K. A. Munro, E. E. McBride, S. R. Evans, H.-P. Liermann, and M. I. McMahon, Phys. Rev. B **90**, 214105 (2014).
[16] W. H. Zachariasen, Proc. Natl. Acad. Sci. USA **75**, 1066 (1978).
[17] Y. C. Zhao, F. Porsch, and W. B. Holzapfel, Phys. Rev. B **50**, 6603 (1994).
[18] R. J. Husband, I. Loa, K. Munro, and M. I. McMahon, J. Phys.: Conf. Ser. **500**, 032009 (2014).
[19] G. N. Chesnut and Y. K. Vohra, Phys. Rev. Lett. **82**, 1712 (1999).
[20] F. H. Ellinger and W. H. Zachariasen, Phys. Rev. Lett. **32**, 773 (1974).
[21] G. S. Smith and J. Akella, J. Appl. Phys. **53**, 9212 (1982).
[22] G. N. Chesnut and Y. K. Vohra, Phys. Rev. B **61**, 3768(R) (2000).

[23] S. Endo, H. Sasaki, and T. Mitsui, J. Phys. Soc. Jpn. **42**, 882 (1977).
[24] Y. K. Vohra and J. Akella, High Press. Res. **10**, 681 (1992).
[25] See Supplemental Material at http://link.aps.org/supplemental/10.1103/PhysRevB.100.024107 for additional information on the issues with the previous x-ray data, and discussions of the relationship among the $oF16$, $oF8$, and $mC4$ structures, which includes Refs. [47–53].
[26] N. C. Cunningham, W. Qiu, K. M. Hope, H.-P. Liermann, and Y. K. Vohra, Phys. Rev. B **76**, 212101 (2007).
[27] T. S. Sokolova, P. I. Dorogokupets, A. M. Dymshits, B. S. Danilov, and K. D. Litasov, Comput. Geosci. **94**, 162 (2016).
[28] A. P. Hammersley, S. O. Svensson, M. Hanfland, A. N. Fitch, and D. Hausermann, High Press. Res. **14**, 235 (1996).
[29] V. Petricek, M. Dusek, and L. Palatinus, Z. Kristallogr.-Cryst. Mater. **229**, 345 (2014).
[30] The space group of the $hP3$ phase of Sm was originally reported as $P3_121$ with atoms on the $3a$ site at $(x, 0, \frac{1}{3})$ with $x = 0.45$ and $c/a = 2.36$ [17]. To date, the $hP3$ structure has been regarded as a distortion of fcc, and the two would be equivalent if $x = \frac{1}{3}$ and $c/a = 2.45$ [17]. More recently, however, using Rietveld refinement, Husband *et al.* reported that $x = 0.513(5)$ [18]. Chen *et al.* have noted that, if $x = \frac{1}{2}$, then the symmetry of the $hP3$ structure becomes $P6_222$ [34]. As this structure has different systematic absences from $P3_121$, these can be used to distinguish the two stuctures. Reanalysis of the data reported in Husband *et al.* [18] reveals that the absences are, indeed, consistent with space-group $P6_222$ rather than $P3_121$, and hence, $x = \frac{1}{2}$.
[31] J. Song, W. Bi, D. Haskel, and J. S. Schilling, Phys. Rev. B **95**, 205138 (2017).
[32] Y. Deng and J. S. Schilling, Phys. Rev. B **99**, 085137 (2019).
[33] Y. Akahama, H. Fujihisa, and H. Kawamura, Phys. Rev. Lett. **94**, 195503 (2005).
[34] Y. Chen, Q.-M. Hu, and R. Yang, Phys. Rev. Lett. **109**, 157004 (2012).
[35] G. K. Samudrala, G. M. Tsoi, and Y. K. Vohra, J. Phys.: Condens. Matter **24**, 362201 (2012).
[36] J. Akella, S. T. Weir, Y. K. Vohra, H. Prokop, S. A. Catledge, and G. N. Chesnut, J. Phys.: Condens. Matter **11**, 6515 (1999).
[37] G. N. Chesnut, Ph.D. thesis, The University of Alabama at Birmingham, 2001.
[38] G. Kresse and D. Joubert, Phys. Rev. B **59**, 1758 (1999).
[39] J. P. Perdew, K. Burke, and M. Ernzerhof, Phys. Rev. Lett. **77**, 3865 (1996).
[40] E. Plekhanov, P. Hasnip, V. Sacksteder, M. Probert, S. J. Clark, K. Refson, and C. Weber, Phys. Rev. B **98**, 075129 (2018).
[41] M. C. Payne, M. P. Teter, D. C. Allan, T. A. Arias, and J. D. Joannopoulos, Rev. Mod. Phys. **64**, 1045 (1992).
[42] S. J. Clark, M. D. Segall, C. J. Pickard, P. J. Hasnip, M. I. J. Probert, K. Refson, and M. C. Payne, Z. Kristallogr.-Cryst. Mater. **220**, 567 (2005).
[43] D. D. Koelling and B. N. Harmon, J. Phys. C: Solid State Phys. **10**, 3107 (1977).
[44] J. Lim, G. Fabbris, D. Haskel, and J. S. Schilling, J. Phys.: Conf. Ser. **950**, 042025 (2017).
[45] M. Petersen, J. Hafner, and M. Marsman, J. Phys.: Condens. Matter **18**, 7021 (2006).
[46] L. W. Roeland, G. J. Cock, F. A. Muller, A. C. Moleman, K. A. McEwen, R. G. Jordan, and D. W. Jones, J. Phys. F: Met. Phys. **5**, L233 (1975).
[47] G. K. Samudrala and Y. K. Vohra, J. Phys.: Conf. Ser. **377**, 012111 (2012).
[48] Y. K. Vohra, B. R. Sangala, A. K. Stemshorn, and K. M. Hope, MRS Proc. **1104**, 1104-NN01 (2008).
[49] G. K. Samudrala, S. A. Thomas, J. M. Montgomery, and Y. K. Vohra, J. Phys.: Condens. Matter **23**, 315701 (2011).
[50] J. M. Montgomery, G. K. Samudrala, G. M. Tsoi, and Y. K. Vohra, J. Phys.: Condens. Matter **23**, 155701 (2011).
[51] D. Errandonea, R. Boehler, B. Schwager, and M. Mezouar, Phys. Rev. B **75**, 014103 (2007).
[52] G. K. Samudrala, G. M. Tsoi, S. T. Weir, and Y. K. Vohra, High Press. Res. **34**, 385 (2014).
[53] A. Togo and I. Tanaka, Scr. Mater. **108**, 1 (2015).
[54] S. Finnegan, E. J. Pace, M. Stevenson, S. G. Macleod, and M. I. McMahon (unpublished).